ELSEVIER

Contents lists available at ScienceDirect

# Journal of Environmental Radioactivity

journal homepage: www.elsevier.com/locate/jenvrad



# Airborne radiometric data: in search of the lost peatlands, Anglesey, North Wales

David Beamish\*, James C. White

British Geological Survey, Keyworth, Nottingham, NG12 5GG. UK

#### ARTICLE INFO

Keywords: Airborne Gamma ray Radiometric Attenuation Soil Peat

#### ABSTRACT

Soil carbon plays a crucial role in maintaining soil health, regulating water retention, and overall ecosystem function, while also acting as a carbon sink that can mitigate climate change. Updating peat information has become a priority in relation to carbon accounting. Soils attenuate radiometric flux by virtue of their bulk density and water saturation. The largest contrasts are associated with high carbon, wet peat zones. A revised attenuation theory demonstrates the response continuum of all soils and defines their response over the full range of saturation levels. The theory can be applied to any form of radiometric survey data. The relevance of the attenuation properties of airborne radiometric data to peat mapping is well established. Mainly due to survey height, the spatial resolution of the radiometric data is limited. It has been argued that conventional peat mapping has omitted many potential areas of peat, often excluded on the basis of depth. These smaller pockets of the carbon store have been termed the lost peatlands. A new observational and adaptable assessment of the peat extent across Wales has recently been published. An existing small airborne survey is used to provide an attenuation assessment of peat extents in relation to the control provided by the new map. Many of the peat zones are small (<0.05 km<sup>2</sup>) and are detected on only one or two flightlines. The large support volume (footprint) of airborne measurements provides a moving-average of subsurface contributions. Despite this, the attenuation response appears sufficient to either confirm or reject the evidence of a peat zone. The data also suggest many other areas of potential peat.

# 1. Introduction

Radiometric attenuation studies related to soil properties exist at a wide range of scales. The most detailed are laboratory techniques which use an active source such as <sup>137</sup>Cs applied to each soil sample. A literature review by Pires (2018) notes the accuracy achieved can be used to determine soil bulk density and water content, along with many other subsidiary properties. At larger scale, due to the rapid increase of soil carbon measurements in relation to soil health and carbon sequestration, England and Viscarra Rossel (2018) presented a field-deployable system (to minimise laboratory costs) that involves an active radiometric source to determine soil bulk density. Proximal passive radiometric surveys are undertaken using a near-source, roving sensor. With a typical height of <1 m, they often provide detailed infill in relation to more limited soil sampling (the control points). Such systems are now used commercially at the farm scale in precision agriculture (Rhymes et al., 2023) and have significance in relation to the push towards agricultural carbon credits. Typically, the attenuation behaviour does not form part of the reported soil assessment.

Drone radiometric systems that can operate at heights of tens of metres have been developed and are now commercially available. Alt-felder et al. (2024) provide a joint drone and ground study noting the resolution issues that come into play with the increase in altitude.

The largest separation between source and passive radiometric detection is embodied in airborne geophysical systems which are typically operated at elevations much greater than 50 m. These systems, invariably deployed in multi-sensor acquisition set-ups, are intended for both shallow and deep subsurface exploration and have been employed for many decades. They inherently provide the lowest resolution of the systems discussed above. Benefits of the existing exploration data sets lie in their uniform spatial coverage involving local, regional and countrywide extents. The more modern (21st Century) data sets are usually undertaken at closer flight line separations and, where permitted, lower elevations.

Here, we consider a small data set of about 6000 line-km acquired with a line separation of 200 m and an along line sampling rate of 60 m.

E-mail addresses: dbe@bgs.ac.uk (D. Beamish), jame3@bgs.ac.uk (J.C. White).

<sup>\*</sup> Corresponding author.

The data were intended for both resource and environmental investigations and here we perform a study of attenuation effects primarily related to soil bulk density (and associated carbon content) and water saturation

Our main focus is how such data may be used to support attempts to revise peat inventories at the regional (or potentially national) scale. They do this by confirming, or otherwise, existing and updated databases that provide evidence of peat and its extent. The data may also suggest potential new, previously unrecognised, areas of peat. The scale at which this achieved is a function of the sampling (e.g. line spacing) of the airborne data together with the survey altitude which determines the contributing volumetric extent, termed the support volume, of each measurement. The height of the measurement is a controlling factor and it is this that distinguishes airborne measurements from those that are proximal to the ground surface. The data were acquired across Anglesey (Ynys Môn), North Wales in 2009 (White and Beamish, 2010). The study area location is provided in Supplementary Material (Fig. SM1).

The term 'the lost peatlands' was coined in an IUCN (International Union for Conservation of Nature) UK Peatland Programme document (IUCN, 2023). The document gives a historical account of the use of the different depth criteria used to classify a soil unit as peat (with a specific focus on the UK). It follows that the use of different criteria may give rise to different estimates of peat extent and volume. Typically, peats with a thickness of <40 cm are excluded, an important consideration for policy initiatives such as carbon emissions reductions, natural flood management and biodiversity targets. The report makes specific reference to shallow (<40 cm) peats as 'thin', 'wasted' and 'peaty pockets' (see also JNCC, 2011). Using a wide variety of data sources, the authors note a UK total of 2,863,826 ha estimate for peat extent using minimum thresholds, compared with a total area of 7,384,544 ha if these minimum thresholds are not applied (IUCN, 2023). More widely, the complex issue of defining and also redefining 'peat' is also discussed by Lourenco et al. (2023) in relation to the development of national scale peat inventories. We note that the airborne data have a well-known sensitivity to the soil properties in the upper 40 cm.

One of the main motivations of the present study was the publication and data release of a new Unified Peat Map of Wales, UPMW, (Welsh Government, 2022). Two data layers were created on a 50 m grid whereby the presence (evidence) and thickness of peat are estimated from a wide-range of observational sources for each grid cell across Wales. The work is a considerable achievement given the observations extend for over a century in time and across a very disparate range of sources. A peatland evidence score defines the level of confidence in the presence of peat in any given grid cell. Using a scoring level protocol, unified polygons are then created across the evidence cells to generate the UPMW. The conventional (pre-UPMW) soil maps across our survey area identify just 4 peat polygons compared with 162 polygons in the new UPMW. The term 'conventional' refers to existing information on peat from the soil mapping of England and Wales and is described later in Section 3.6. The vast majority (128) of the 'new' peats are small zones with areas <0.05 km<sup>2</sup> (5 ha). The zones therefore constitute 'lost' peats e.g. small peaty pockets previously unrecognised in existing carbon accounting. In geophysical terms, the zones high-wavenumber components of the data set.

The UPMW data are used to provide interpretation control of the many localised attenuation zones observed across our study area. By spatial colocation we are then confident that the attenuation zones relate to a peat response. Although we display the thickness information, it is not used directly in our assessment/interpretation due to the moving-average nature of the airborne measurement. The detailed comparisons undertaken allow the various resolution limitations of the airborne data to be demonstrated.

In this paper, we first provide an outline of radiometric attenuation behaviour in soils, followed by a summary of the data sets utilised in this study. Subsequently, we introduce key interpretation techniques for analysis of airborne data and then present regional scale findings alongside detailed targeted studies.

#### 2. Revised (simplified) attenuation theory

In previous attenuation studies it was found difficult to summarise the radiometric attenuation behaviour as a function of soil bulk density due to the additional interplay of water content (saturation) and porosity (voids). Beamish (2013, 2014) summarised the behaviour of indicative soil types using assumed levels of porosity. It was noted that it was highly unlikely that the assumed porosity is applicable across all the soil types considered. It is possible to extend and simplify the approach adopted by Beamish (2013) if we note that the bulk density ( $\rho_b$ ) is related to porosity ( $\Phi$ ) as:  $\Phi=1-(\rho_b/\rho_s)$  where  $\rho_s$  is the particle density (Reynolds et al., 2020).

Following the early work of Adams (1973), the significance of SOM (Soil Organic Matter) content and particle density, as fundamental properties of all soils, has been developed in numerous studies (Rühlmann et al., 2006; Périé and Ouimet, 2008). Using mixture theory, it is common to partition the soil material into mineral and organic fractions using particle density end members for mineral and organic soils (see below). The partitioning approach can be used to examine the attenuation sensitivity of the radiometric response to both bulk density and SOM across the whole range of soil types.

Since there are a wide number of formulations of soil-SOM relationships in the literature, we use the recent partition expressions given by Robinson et al. (2022) to provide relationships for radiometric attenuation based on bulk density and SOM. We use equation (1) of Robinson et al. (2022), which defines the combined bulk density of soil with mineral (M) and organic matter (OM) components as, (using the same nomenclature):

$$\rho_b = 1 / \left[ \frac{SOM}{\rho_{bOM}} + \left( \frac{1 - SOM}{\rho_{bM}} \right) \right]$$
 (1)

where bulk densities are in g.cm $^{-3}$  and SOM is a fractional percentage (0–1). The equation requires the 'pure' end-member densities of organic matter ( $\rho_{bOM}$ ) and mineral matter ( $\rho_{bM}$ ). Robinson et al. (2022) demonstrate the effective use of the values  $\rho_{bOM}=0.09$  and  $\rho_{bM}=1.94$  g cm $^{-3}$ .

Porosity ( $\Phi$ ) is then defined by equation (2) of Robinson et al. (2022) as:

$$\varnothing = 1 - \left[ \left( \frac{SOM}{\rho_{sOM}} + \frac{1 - SOM}{\rho_{sM}} \right) / \left( \frac{SOM}{\rho_{bOM}} + \frac{1 - SOM}{\rho_{bM}} \right) \right]$$
 (2)

where  $\rho_{sM}$  and  $\rho_{sOM}$  are the intrinsic particle densities of mineral and organic material, respectively. The authors then use the data on particle densities provided by Rühlmann (2020) to determine the particle density for end members of mineral ( $\rho_{sM}=2.7~g~cm^{-3}$ ) and organic ( $\rho_{sOM}=1.4~g~cm^{-3}$ ) soils. Using the 2 equations we are able to define the linear relationship between porosity and bulk density and the highly non-linear relationship between bulk density and SOM. These are both shown in Supplementary Material (Fig. SM2). The SOM may be converted to an estimate of soil organic carbon (SOC) by using a conversion reduction factor that may range from 43 to 58 % (ADAS, 2019) with a typical value of around 50 % (Lindsay, 2010).

Here we use porosity as defined in equation (2) and obtain the attenuation as a function of bulk density and SOM for specific values of saturation. It is worth noting that radiometric attenuation is necessarily defined as a relative change in count rate (radiometric flux) so that here, as previously, attenuation of a given spectral component is referenced to a material of the same bulk density with no water content. The formulation uses soil saturation which is a volumetric measure of soil moisture; soil moisture based on sampling and laboratory analysis is usually quoted as a gravimetric (weight based) measure of water content.

The radiometric flux attenuation is obtained using the method of Beamish (2013) for values of bulk density from almost 0 to 2 g cm $^{-3}$  and

the associated values of fractional SOM in the range 0–1. The results are cycled through a range of soil saturation levels that are responsible for the flux attenuation. Fig. 1a shows the resulting attenuation sensitivity in the familiar framework of bulk density. The corresponding result in the framework of SOM is shown in Fig. 1b. The 3 zones of soil type (organic, organo-mineral and mineral) are based on typical bulk densities found in the literature and are indicative rather than absolute. The significance of the new results is that when examining different attenuation levels across peat zones and their adjacent soils we no longer have to consider soil porosity as part of the assessment. We can also note that the laboratory measurement of soil porosity, as a function of soil-type, is not common.

The results of Fig. 1 demonstrate the >90 % attenuation associated with low density peat soils for saturations >60 %. Realistic peat saturations are typically >90 % and are distinct from other soils. The behaviour observed also indicates a low sensitivity to changes in bulk density (<0.4 g cm<sup>-3</sup>) at these high saturations. It is unlikely that the data could distinguish a peat soil from a 'peaty' (higher bulk density) soil. In other soils the most sensitive attenuation behaviour is observed through the organo-mineral transition to mineral soils. Using a 40 % saturation and a reference bulk density of 1 g cm<sup>-3</sup>, the relative attenuation of a soil with a bulk density of 1.6 g cm $^{-3}$  is a decrease of -23 %and for a soil of bulk density  $0.5 \text{ g cm}^{-3}$  it is an increase of +35 %. Similar values are obtained at 60 % saturation (-26 % and +32 % respectively). Given accurate data, such relative variations in bulk density may be detectable if the property contrast is high and the airborne measurement scale is appropriate. It is worth noting that a lower bound on soil moisture for UK soils was considered by Beamish (2015). Across the study area (Anglesey), the lower bound for many non-peat soils may be in the range 25-35 %.

The main interpretation issue, for all soils, is the duality of the radiometric attenuation response (referred to here as BD-SAT). If bulk density (BD) were known, significant soil saturation (SAT) contrasts may be detected, and vice-versa. The control information required to separate out the response duality at the scale of the airborne measurement is generally not available. As noted later in our Discussion section, the estimation of soil water saturation levels is an active research topic and was briefly considered for the present study area. Since no firm outcomes were established, the results of Fig. 1 are presented to point the way towards further studies.

#### 3. Materials

In this section we first introduce the 2 key data sets used in our assessments which are the airborne radiometric survey data and the Unified Peat Map of Wales (UPMW). The geological setting and soils which both contribute to the radiometric response are then described at the large scale. Subsidiary data sets used in the interpretation include Lidar (Digital Terrain Model 'DTM'), water courses and topographic map information.

#### 3.1. The airborne survey

Our study considers the radiometric data acquired during an airborne survey over the island of Anglesey (Ynys Môn), North Wales. The survey area shown in Supplementary Material (Fig. SM1) encompasses the whole island and a coastal strip on the Welsh mainland (1198 km²). The survey was carried out between 12th and June 18, 2009. Over 6000 line-km of data were acquired using a fixed-wing DHC-6/300 Twin Otter. Beamish and White (2009) and White and Beamish (2010) describe the acquisition and processing procedures; the former reference provides details of the instrumentation. 223 parallel flight lines were flown, in a N-S direction, in order to cross-cut the dominant geological trends (NE-SW and NW-SE). All the data were acquired and processed in the British National Grid (BNG) coordinate system (EPSG:27700).

The survey was conducted at high resolution (a flight line spacing of 200 m) and at low altitude (a survey median value of 54 m) rising locally in the vicinity of conurbations and the main cross-country power lines. The three main data sets acquired were magnetic, radiometric (gamma ray spectrometry) and active frequency domain electromagnetic (EM). The along-line radiometric data were sampled at a fairly constant interval of 60 m (1 sample per second). The data were gridded using a minimum curvature algorithm to provide a grid cell size of 50 m. These grids form the main data set used here. Beamish and Schofield (2010) provide an overview of the motivation and results of the survey in the context of resource and environmental applications of the 3 data sets. Here we consider only the radiometric data. The Anglesey survey data may be requested from the enquiry service at the British Geological Survey (enquiries@bgs.ac.uk).

#### 3.2. The radiometric data

A full account of the standard processing applied to the data is given

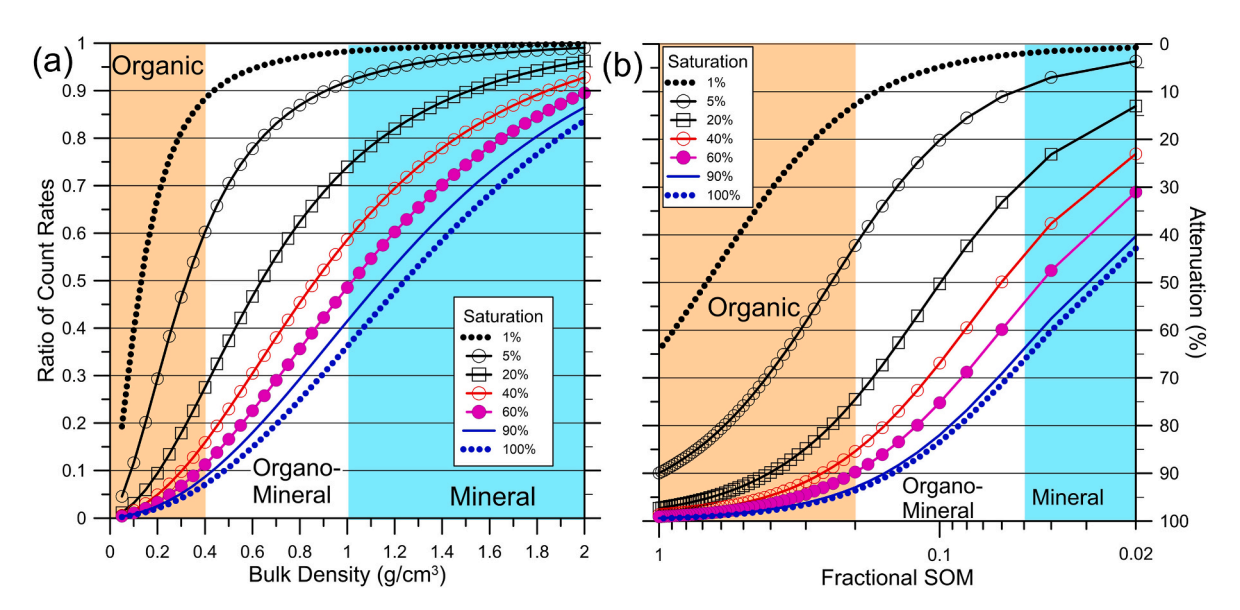


Fig. 1. Flux attenuation as a function of (a) dry bulk density and (b) fractional SOM, for a range of soils and water saturations. The 3 zones of soil type are based on typical bulk densities and are indicative rather than absolute.

in White and Beamish (2010). The data considered here are count rate data (flux in counts per second 'cps') converted to apparent concentrations in the 3 radioelements Potassium (K), Thorium (Th) and Uranium (U). The procedure determines the concentrations that would give the observed count rates, if uniformly distributed in an infinite horizontal source. Because the U and Th windows actually measure <sup>214</sup>Bi and <sup>208</sup>Tl respectively, the calculation implicitly assumes radioactive equilibrium in the U and Th decay series. The U and Th concentrations are therefore expressed as equivalent concentrations, eU and eTh. The Total Count is the total count observed within the recommended (IAEA, 2003) energy range 0.41–2.81 MeV which contains the contributions from all 3 radioelements and is expressed in cps.

The area covered by the airborne survey (Fig. SM1) contains a significant extent of seawater. We clipped the data grid to the coast to evaluate only the onshore domain. In summer there may be a tidal range of about 6 m across the island and here we present data extending to the defined low water mark to include all potential effects from inter-tidal coastal zones. The water column will typically provide attenuation scale lengths of between 40 cm (90 %) and 80 cm (99 %) (Beamish and White, 2024, Fig. 1a). In some shallow (<40 cm) water circumstances the flux from the underlying sediments can be observed.

#### 3.3. The study area and DTM

As noted previously, the radiometric data were cut to the low water mark to evaluate the maximum extent of the onshore area. The large scale DTM across the rectangular frame of our data presentations is shown in Fig. 2. The island presents a low-lying topography with generally undulating features. There are a number of localised basement peaks and ridges in excess of 120 m. The coast, particularly in the SW, contains a range of intertidal zones (elevations <5 m). These present a

considerable challenge to radiometric peat detection due to potentially high water-saturation levels. The Menai Strait (Fig. 2) has an interesting peat association. Roberts et al. (2011) describe marine-cores from NE Menai Strait that found a sequence of multiple peat/organic horizons interbedded within the thick estuarine–marine sequence. <sup>14</sup>C dating of the peat indicated initial breaching of the Menai Strait between 8.8 and 8.4 ka BP to form a tidal causeway, with final submergence between 5.8 and 4.6 ka BP. The shading of the DTM relief reveals a number of large-scale striations (scourings) formed by the last (Devensian) glaciation and subsequent ice stream retreat. We also show an extensive glacial drumlin field (localised topographic ridges) in transparent grey. These are discussed in relation to superficial deposits below.

Fig. 2 introduces 4 zones, shown by labelled solid rectangles (1–4), which are used for detailed studies of peat detection. In addition, dotted rectangle A encompasses the largest conventional peat deposit on Anglesey (Cors Erddreiniog). Rectangles A and 3 form part of the Anglesey Fen wetlands which were studied using both radiometric and EM data sets by Beamish and Farr (2013). Rectangle B is centred on Parys Mountain and is used only to note the radiometric response to mineralisation.

#### 3.4. The Unified Peat Map of Wales (UPMW)

One of the main motivations of this study was the publication and data release of a new (updated) unified peat map of Wales. In order to support policy decisions and inventories, revisions to existing maps and data on peat have accelerated, often using new adaptive protocols when combining information from the many disparate organisational sources. A number of such revisions, such as that for Ireland (Gilet et al., 2024), have recently become available. Here we consider the new unified peat map of Wales and use a small portion of it in relation an airborne survey

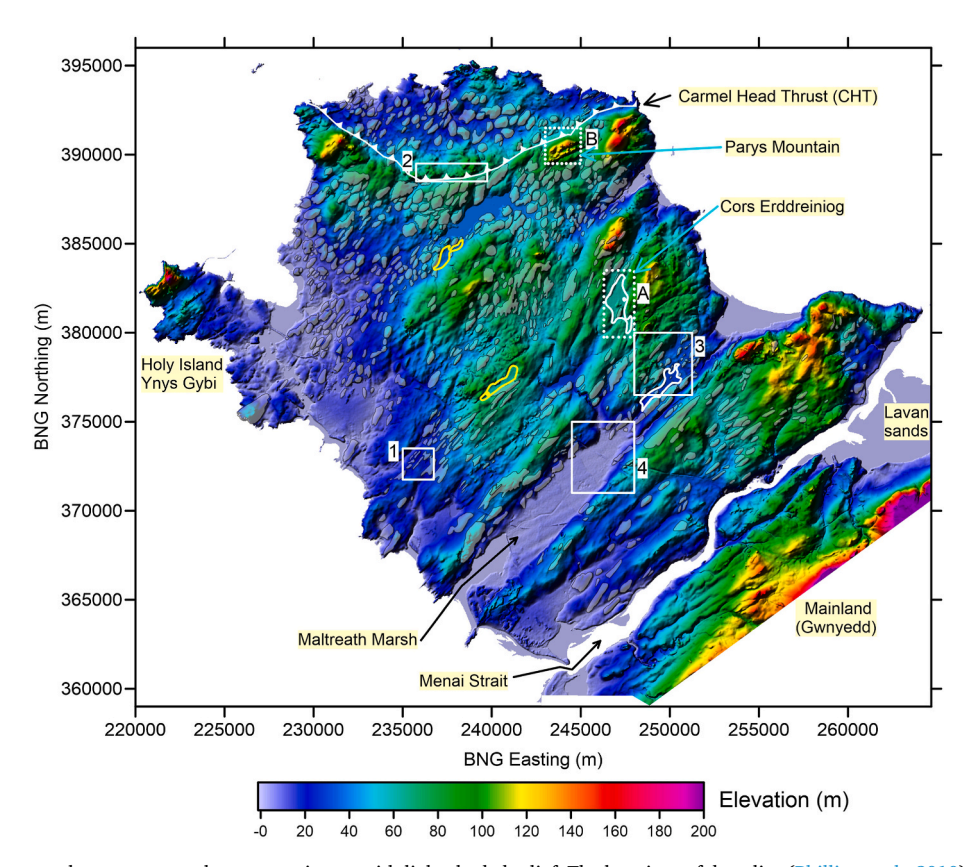


Fig. 2. Large scale DTM across the survey area shown as an image with light shaded relief. The locations of drumlins (Phillips et al., 2010) are shown in transparent grey. Two Fen peats (white) and two blanket peats (yellow), obtained from conventional soil mapping. Also shown are the locations of detailed study rectangles as solid lines (Areas 1–4) and also 2 rectangles (A, B) with dotted lines. These are discussed in the text. (For interpretation of the references to colour in this figure legend, the reader is referred to the Web version of this article.)

across the island of Anglesey, North Wales.

The data were obtained from the government of Wales website: https://datamap.gov.wales/maps/peatlands-of-wales-maps/. The provision of the data is via an Open Government Licence for Public Sector Information. The data provide the distribution of Welsh Peatlands (to 2022) based on updated evidence sources. The data layers were created on a 50 m grid whereby the presence and thickness of peat are estimated from a wide-range of *observational* sources for each 50 m grid cell across Wales. The outputs are presented as 3 data layers (i) peat evidence score (EVIDENCE), (ii) peat thickness (THICKNESS) and (iii) Unified peat (UNIFIED), as shown in Table 1.

The information is intended to be used as a 'living map', where a 50m grid can be updated with new information when it becomes available through monitoring, surveys and measurements of peat presence. The present study therefore forms part of the intended framework. Since the main procedure used evidence for deep ( $>40~\rm cm$ ) peats an initial (top) layer thickness (actually 0–42 cm in the supplied data set) may be considered a 'residual' upper estimate of the protocol.

## 3.5. Geological setting

The geology and tectonic framework of Anglesey is complex and a full description is beyond the scope of the present study. The present geological configuration can be understood in terms of a tectonic amalgamation of terranes. Central Anglesey can be considered a microcontinent with ancient subduction zones to the NW and SE. More detailed and relevant bedrock and superficial geological descriptions across the study area are presented by Beamish and White (2011), White and Beamish (2014) and Phillips et al. (2010). The lithological units encountered are assumed to provide the parent radionuclide material to the derived soils and superficial units. Here the 1:250k scale digital bedrock geology (British Geological Survey, 2005) is used as the basis for a lithological classification. The mapping provides a unique RCS (Rock Characterisation Scheme) defining 16 distinct lithological units, described in Supplementary Material (Table SM1). The tectonic structures and faults on Anglesey are significant but here we make reference to just one major feature. The Carmel Head Thrust (CHT) is a major Caledonian thrust plane in which older Precambrian rocks (in the north) have been thrust over younger Ordovician shales (to the south). This arcuate zone traverses the Parys Mountain mine site (rectangle B, Fig. 2) which is interpreted to be a volcanic-hosted massive sulphide (VMS) zone containing significant polymetallic zinc, copper, lead, silver and gold deposits. Since VMS deposits can be assessed using radiometric data (Morgan, 2012) we overview the data across the existing mine site.

The RCS bedrock map is shown in Fig. 3a. This can be compared with the survey data presented as a ternary image that summarises the relative K, Th and U radioelement contributions (Fig. 3b). The colour zones tending to white denote high emissions in all three radioelements and the zones tending to black denote low emissions in all three radioelements. At the large (long wavelength) scale there are a number of clear associations between the bedrock lithologies and radiometric characteristics. The Carboniferous limestones (LMST) are clearly enhanced in Uranium. The Y-shaped northern zone (AROC) defines Ordovician sediments enhanced in Thorium and higher flux. To the north, bounded by

**Table 1**UPMW layers defining confidence in the presence of peat.

| Layer     | Details  | Assessment<br>Score/Criteria | Resolution  |
|-----------|--|------------------------------|---|
| EVIDENCE  | Confidence in the presence of peat               | 1–9                          | 50 m grid   |
| THICKNESS | Estimate of peat thickness                       | Thickness in cm              | 50 m grid   |
| UNIFIED   | Presence of peat<br>(where EVIDENCE<br>layer >1) | Yes/No                       | Set of polygons<br>extracted from<br>EVIDENCE LAYER |

the CHT, are Precambrian rocks (Neoproterozoic III) which have been thrust over the younger sediments to the south. These ancient lithologies present a uniform 'mottled' appearance. Of more relevance to our present study are the flux attenuation zones presenting darker colours. The intertidal zones are clearly defined as are the many onshore water bodies and larger peat bodies (e.g. rectangle A). At the detailed (high wavenumber) scale, there are a plethora of instances of localised high attenuations which, as demonstrated later, are the peats which form our study targets.

Throughout substantial periods of the Devensian Glaciation, the UK and Ireland were covered by the British and Irish Ice Sheet (Phillips et al., 2010). Anglesey was coincident with the Irish Sea Ice Stream which served to create the distinctive NE-SW surface features seen today. Several zones on Anglesey display major sub-glacial deposition in the form of extensive drumlin fields as shown in Fig. 2. The drumlins themselves are defined by a topographic (raised) form but their internal architecture may vary massively with structures ranging from thick till layers to very thin till deposits overlying a bedrock core. The till itself comprises angular bedrock pieces in a sandy to muddy matrix; it is thought to be representative of the underlying geology (Phillips et al., 2010). The drumlins have an average length and width of approximately 1 x 0.25 km. White and Beamish (2014) undertook a study of the EM (resistivity) survey data in relation to the drumlin field and detectable but variable drumlin effects were observed. Here, by way of contrast, we find no detectable radiometric responses that can be ascribed to the drumlin field, either at the individual or larger scales.

#### 3.6. Soils

The conventional soil map of England and Wales, including Anglesey, is based on a 'named' convention of the soil series. On Anglesey there are 2 peat series named Crowdy (Blanket peat) and Adventurers' (Fen peat). There are two areas associated with each of the two series which are identified in Fig. 2. UK soil property information at the national scale is currently supplied by a soil observatory server (http://mapapps2.bgs.ac.uk/ukso/home.html) which contains both soil and soil-parent material information. One available product is the simplified Soilscape database (Farewell et al., 2011) which is a reclassification of the conventional soil series. The spatial configuration of soil units across the study area can be viewed online using the link provided above. The classification scheme adopted is, however, intended for the generalist user. As such it does not support an understanding of the variation in typical soil bulk densities required in the assessment of the radiometric response as shown in Fig. 1.

## 3.7. Lidar

Lidar topographic data (1 m resolution) for the whole of Wales are available from the Government of Wales data server at <a href="https://datamap.gov.wales/maps/lidar-data-download/">https://datamap.gov.wales/maps/lidar-data-download/</a>. Both DSM and DTM (bare Earth) data are available. The provision of the data is via an Open Government Licence for Public Sector Information.

### 3.8. Water courses (NRW)

NRW water course data for the whole of Wales are available from the Government of Wales data server at <a href="https://datamap.gov.wales/layers/inspire-nrw:NRW\_MAIN\_RIVERS">https://datamap.gov.wales/layers/inspire-nrw:NRW\_MAIN\_RIVERS</a>. The provision of the data is via an Open Government Licence for Public Sector Information, which can be viewed on the link provided (Read more about this licence).

#### 3.9. Ordnance Survey maps

For the detailed studies we use Ordnance Survey (OS) 1:50k colour topographic raster maps (Landranger). These are information rich and contain: (i) Topographic height contours at 10 m intervals (light brown).

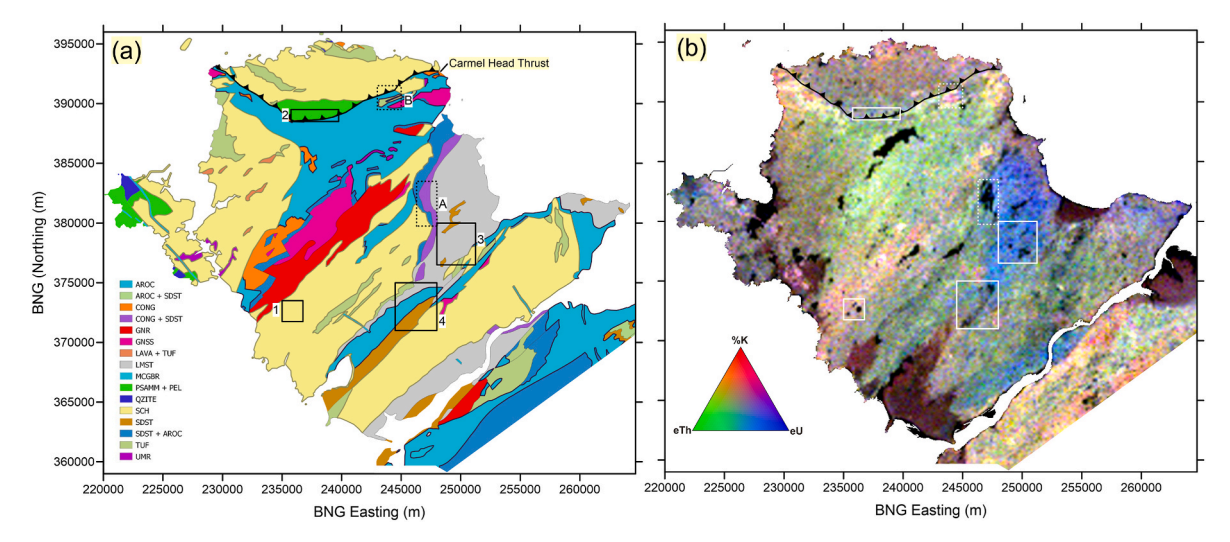


Fig. 3. (a) The distribution of bedrock lithologies (1:250k scale) across the survey area. The Rock Characterisation Scheme (RCS) is described in Table SM 1. (b) The ternary image obtained using the 3 radioelements. Both panels show locations of detailed study rectangles as solid lines (Areas 1–4) and also 2 rectangles (A, B) with dotted lines.

(ii) Areas of marsh (tuft symbols in light blue). A marsh is generally understood to be an area of land that is frequently or constantly flooded with water. No particular soil type is implied. (iii) Water bodies (light blue). (iv) Water courses (light blue). These are invaluable for assessing the hydrological connectivity of the area. They are typically more extensive than digital information on water courses. The maps contain OS data © Crown copyright and database rights 2025. OS AC0000824781 EUL.

#### 4. Methods

The relevance of airborne radiometric survey data to peat mapping is now well established. Studies of blanket bogs by Beamish (2013, 2016a) and those across lowland areas (meres, fens and afforested peat) and upland areas of blanket peat (Beamish, 2014) form an existing background. A summary of the basic technical understanding of radiometric attenuation applied to peat is provided in Beamish and White (2024, Section 2). Here, we provide a short summary of the key analysis techniques, applied to airborne radiometric data, that allow spatial mapping of peats.

### 4.1. Data sampling (a moving average)

The equation that relates the contribution to the gamma ray signal in the detector originating from a volume element in the soil is based on Lamberts Law (Duval et al., 1971). The relationship involves an integral equation that is infinite in the distance variable defining the separation of detector and source. It is therefore necessary to describe the support volume of each measurement in terms of percentage contributions. Following Duval et al. (1971) and Pitkin and Duval (1980), Beamish (2016b) presented percentage contributions to the support volume for a detector height of 60 m. This is close to the median height of our survey. The 90 % contribution is a circle of radius 125 m at each sampling point. The 50 % contribution is a circle of radius 37.5 m, and is relatively compact. However, the 90 % contribution to each measurement would be obtained at radial distances of 125 m (a spatial scale of 250 m). We calculate that only every fourth measurement (240 m along line) is independent at the 90 % contribution level in the case of a uniform subsurface. The data acquired at 60 m along line are therefore a moving average (equivalent to a low-pass filter) over these spatial scales. The data recorded are thus a smoothed representation of a potentially discrete zone.

The behaviour is further demonstrated when examining the

radiometric response of a discrete zone of peat as modelled by Beamish and White (2024, Fig. 3). It forms a basic resolution limitation of the technique when airborne data are used at detailed scales. The smoothing is demonstrated throughout the examples presented here. Larger zones do however adopt more realistic geometrical forms in keeping with the control evidence layer.

#### 4.2. Edge detection: The Horizontal Gradient Magnitude (HGM)

The modelling of non-uniform, discrete zones (source contrasts) responsible for both flux attenuation and enhancement was conducted by Beamish (2016b) and Beamish and White (2024). The attenuation and enhanced responses are the inverse of each other (the maximum becomes the minimum and vice versa). The response takes the form of a bell-shaped anomaly with half-widths (50 % reduction in amplitude) ranging from 140 m (circular source with radius of 25 m) to 370 m (circular source with radius of 200 m) when the survey elevation is 60 m (Beamish, 2016b). Another important feature of the response at decreasing scales (radius) of the source is the reduction in maximum amplitude. Using the results obtained at 60 m elevation, the correct amplitude is only observed when the source radius is greater than the line spacing.

Due to the relatively low lateral resolution of the discrete response, Beamish (2016b) introduced one of the edge detection procedures common in geophysical processing. The Horizontal Gradient Magnitude (HGM) is based on the x-derivative (dx) and y-derivative (dy) responses and is defined as the positive-only response:

$$HGM = \sqrt{\left(dx^2\right) + \left(dy^2\right)} \tag{3}$$

Modelling of the HGM response indicated that maxima were associated with the edges of discrete zones and therefore allowed an improved method of detection and definition of each zone of attenuation. Many implementations of spatial gradient calculations use simple first difference formulae and these are adequate when the data are noise-free. It has long been recognised that noise in geophysical data subverts the reliable calculation of the many spatial gradients used in interpretation schemes. Thurston and Brown (1994) introduced a variable pass-band horizontal gradient operator that allows for high frequency (wavenumber) noise to be suppressed. The method is, in fact, a generalisation of the first difference approach. We use this approach here but note that the precise method of filtering used may vary across the data sets considered.

As in previous analyses, we apply curvature analysis to map maxima (ridge) locations in the HGM grid. Phillips et al. (2007) employed a  $3\times3$  (grid cell) moving-window to assess the local curvature and define turning points (e.g. ridges). The local curvature is obtained by fitting a quadratic surface to each of the 3x3 windows and typically will produce some spurious values.

#### 4.3. Edge detection: The local variance filter

In the context of edge detection, we have also found that the Local Variance (LV) filter provides a useful and straightforward means of boundary detection. To assess the *high wavenumber* content of the data we apply a local variance filter using a 3 x 3 grid cell moving window. According to Woodcock and Strahler (1987) local variance is estimated as the mean value of the variance of a moving 3  $\times$  3 window. In a grid, each point (except around the edge) can be considered the centre of a 3  $\times$  3 window. The variance of the nine values is computed in standard fashion by first forming the mean and then determining the local variance. This value is attributed to the central grid cell. Since this is a local estimate, across a 150  $\times$  150 m rectangle in our case, a shaded relief image of the LV estimates is used to highlight the high wavenumber information obtained. The LV estimates provide a simple and robust alternative to the numerical procedure of forming spatial gradients.

#### 5. Results

In this section we provide an initial large-scale overview of the data and some of the significant features within the study area. We then consider detailed studies across the selected areas (solid rectangles 1 to 4, Fig. 2) with regard to the airborne information and their relationships to the 3 layers obtained from the Unified Peat Map of Wales. The section ends with a summary across the whole study area.

#### 5.1. Overview

We investigated the high wavenumber content of all the radiometric data (%K, eTh, eU and TC) using the Local Variance (LV) filter across the survey area. Shaded relief maps of these data are compared in Supplementary Material (Fig. SM3). Although the signal/noise contributions to airborne radiometric data are difficult to separate formally (Billings

et al., 2003), we can compare the clarity of the normalised data LV responses in relation to our requirement to detect small-area responses from potential peat zones. The results suggest that the TC, followed by % K, offer the least noise-prone information. Here we use just the TC data. The eU data appear particularly noisy. We assessed the statistical information in the 4 data sets using a reduced data set to suppress the low values introduced by water. The data were cut to high tide, water bodies were eliminated and further manual cuts were introduced at various coastal locations. This is referred to as the reduced data set. The median values of the reduced data sets were 1.26 (%K), 5.39 (eTh, ppm), 1.09 (eU, ppm) and 2032 (TC, cps). The first two values are within the global average abundances reported by IAEA (2013) while the eU result is much less than the reported range of 2–3 ppm.

The TC data used for the study are shown in Fig. 4a and overlaid with the detailed study rectangles (1-4, A-B) introduced previously. Fig. 4b shows the shaded-relief LV normalised response of the TC data. The largest flux values were recorded over the 2 working extractive quarries (granite aggregate) circled in red. Maximum survey TC values of 4887 cps were observed in the north (Gwyndg Quarry) and 4791 cps in the south (Caer Glaw Quarry). High flux values associated with larger quarries are a common feature of the modern airborne UK surveys. Due to the absence of soil cover we observe the bedrock response (from granite in this case), or at least an approximation to it. Using the reduced data set we are able to estimate a median value of the granite classified TC data (GNR, Fig. 3a) to be 2368 cps. The observed quarry bedrock response is therefore a factor of about 2 above the 'normal' soil attenuated response of granite. The factor of 2 is significant since the same factor was introduced when estimating the radiogenic heat production across the geothermal granite in SW England, in an attempt to supress soil attenuation effects (Beamish and Busby, 2016).

Other high flux values are also recorded to the south of Carmel Head Thrust (CHT) (mainly the western and eastern limbs) within the Ordovician sediments (AROC lithology, Fig. 3). The LV response (Fig. 5b) indicates chaotic (?) structures extending across the Parys Mountain site (rectangle B). It is possible to speculate that these may reflect the near-surface, tectonic 'crumple zone' associated with thrusting and observable at some surface locations. The mainland location labelled F presents a large-scale LV boundary observed at the termination of the Carboniferous lithology as shown in Fig. 3. The boundary is also a regional fault. Finally, we provide two examples of small area, isolated responses

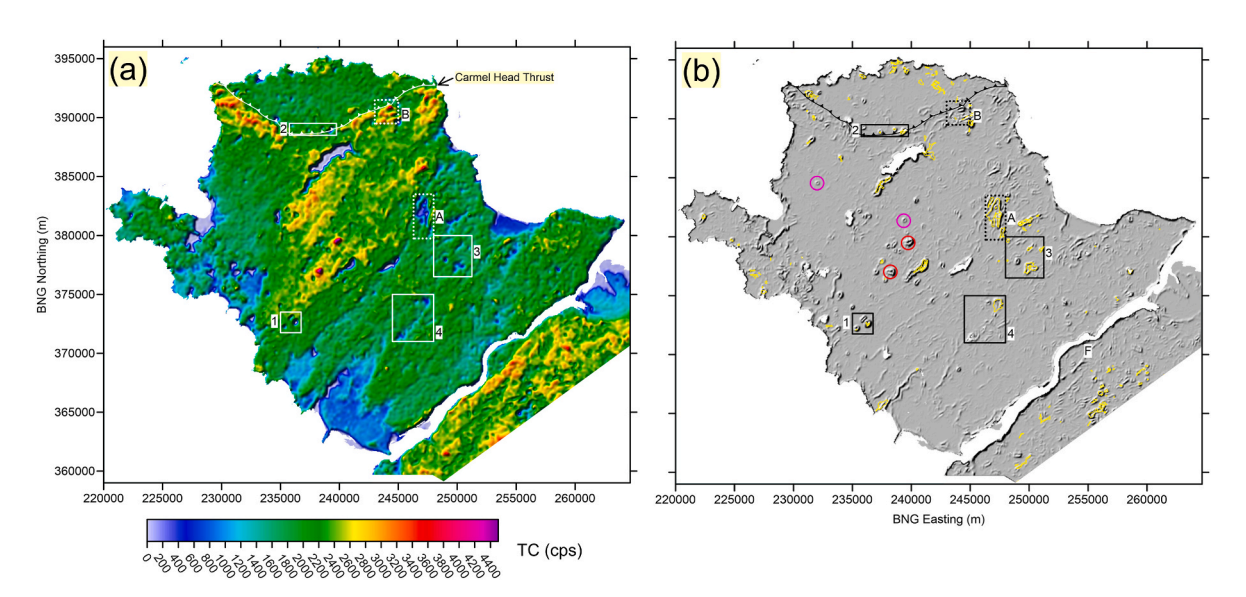


**Fig. 4.** (a) The Total Count (TC) data across the survey area. (b) Shaded relief image of the Local Variance (LV) filter of Total Count, TC, cps. Onshore water bodies in white. The EVIDENCE layer (all scores) from the Unified Peat Map of Wales, in yellow. F = Fault. 4 coloured circles are discussed in the text. Both panels show locations of detailed study rectangles as solid lines (Areas 1–4) and also 2 rectangles (A, B) with dotted lines. (For interpretation of the references to colour in this figure legend, the reader is referred to the Web version of this article.)

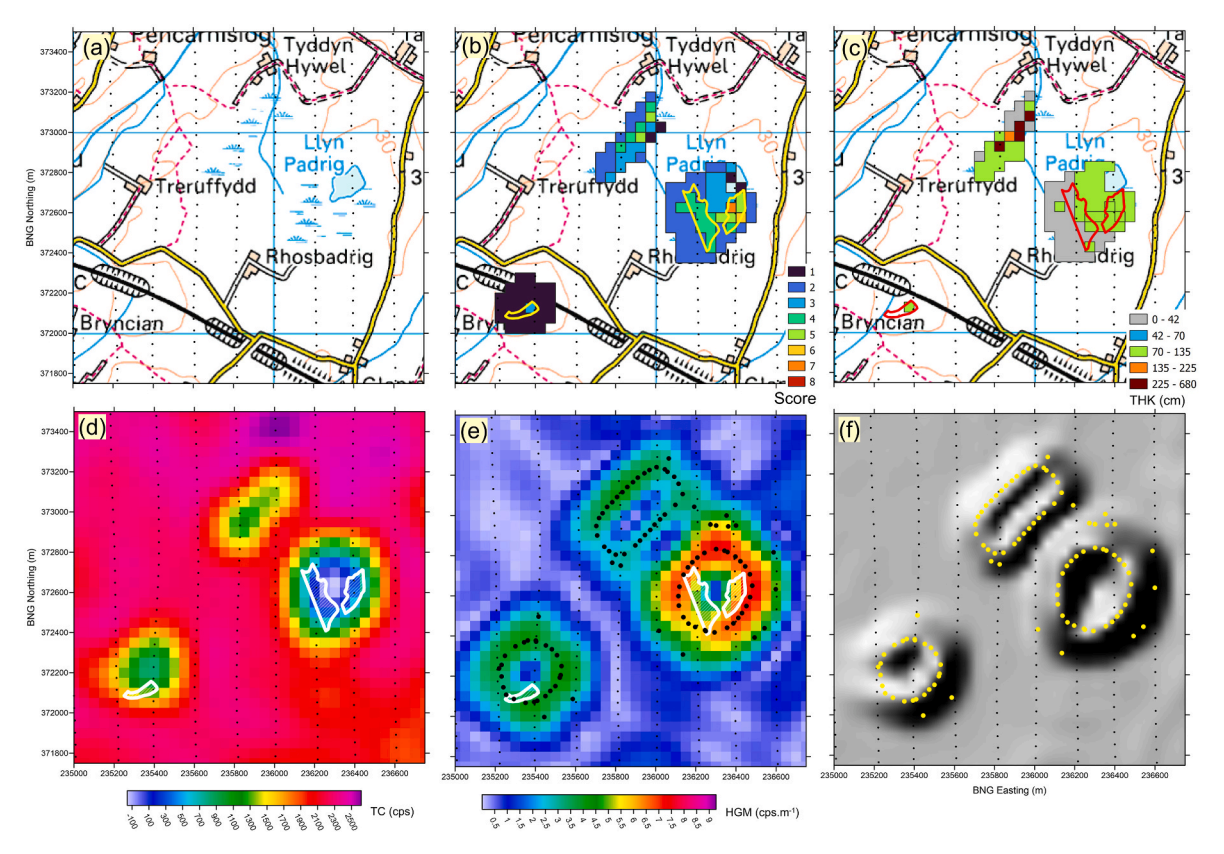


Fig. 5. Area 1, detailed study. (a) OS 1:50k topographic map. (b) With UPMW EVIDENCE layer scores and UNIFIED polygons in yellow. (c) With UPMW THICKNESS (THK) layer and UNIFIED polygons in red. (d) Total Count (TC) 50 m grid and UNIFIED polygons in white. (e) 50 m grid Horizontal Gradient Magnitude (HGM) and curvature ridge solutions (HGM  $\geq$  3 cps.m $^{-1}$ ), black dots. (f) Shaded relief image of the Local Variance (LV) filter of Total Count, TC, cps with HGM curvature ridge solutions, yellow dots, from previous panel. The map contains OS data © Crown copyright and database rights 2025. OS AC0000824781 EUL. (For interpretation of the references to colour in this figure legend, the reader is referred to the Web version of this article.)

(bullseyes) that occur throughout the study area. These are identified by purple circles (Fig. 4b). The circles show typical small area attenuation effects not identified in the Unified Peat Map of Wales.

## 5.2. Detailed studies

As indicated in the summary of Fig. 4, there are numerous instances of high wavenumber attenuation effects in the data. Four, non-exhaustive, detailed comparisons between the airborne data and the UPMW data layers were chosen to allow the various resolution limitations of the airborne data to be demonstrated. The first two areas can be regarded as relatively simple while the second two areas are more complex.

The four detailed examples of Total Count data shown in this section have data ranges specific to each area (to preserve dynamic range). Since this is variable across areas, it is necessary to note the low value TC limit and a value of about of 1500 cps which typically denotes significant attenuation. All the plots show the observation points along each flight line as small dots in the N-S survey direction. Average survey altitudes across the four areas range from 52 to 54 m.

#### 5.2.1. Area 1

The results across the  $1.75 \times 1.75$  km area are assembled in Fig. 5. Fig. 5a shows the base OS 1:50k topographic map as described previously. The area contains one water body and two areas of marsh. Fig. 5b shows the same base map with the UPMW EVIDENCE and UNIFIED polygon layers, the latter being derived from the former using the scores (1–7) shown. Only two of the three zones provide UNIFIED polygons. Fig. 5c shows the THICKNESS layer and again the UNIFIED polygons. Thicknesses extend to >2.25 m. Fig. 5d shows an image of the TC data as

a grid rather than the usual contoured approach. This is in keeping with the 50 m grid used by the UPMW layers but is only used in this first example. Three areas of attenuation are observed in keeping with the EVIDENCE layer. We can therefore associate these areas with peat. The largest area provides a low amplitude of zero while the other two areas are closer to about 1000 cps with an onset of about 1500 cps. As noted previously, from the modelling of small discrete bodies by Beamish (2016b) the correct low (or high) amplitude response is only observed when the source radius is greater than the line spacing. This effect is a likely cause of the behaviour observed. In addition, the inherent moving average (low pass filtering) nature of the data is very evident causing a 'bullseye' effect. Fig. 5e shows the HGM response again as a grid image. This grid is then used in a curvature (ridge) analysis to provide 'best' estimates of the source boundaries as discrete points (in black) obtained at the grid resolution. The boundaries shown use a low value limit of HGM>3 cps m<sup>-1</sup> which is selected based on the amount of spurious behaviour introduced. Fig. 5f shows a shaded-relief image of the LV filter; the HGM boundaries from the previous panel are overlaid. This again demonstrates the utility of this approach to small area detection.

#### 5.2.2. Area 2

The area has dimensions of 4 x 1 km. The results across the area are assembled in Fig. 6. Fig. 6a shows the base OS 1:50k topographic map with 2 water bodies and a single area of marsh. Fig. 6b shows the same base map with the UPMW EVIDENCE and UNIFIED polygon layers. There are five EVIDENCE zones identified together with a single grid cell. Only three of the EVIDENCE zones generate UNIFIED polygons. Fig. 6c shows both an image and contours of the TC data overlaid with the curvature (ridge) solutions obtained from the HGM grid (not shown). Here the ridge solutions are obtained with HGM  $\geq$  2.5 cps m $^{-1}$ . Four of

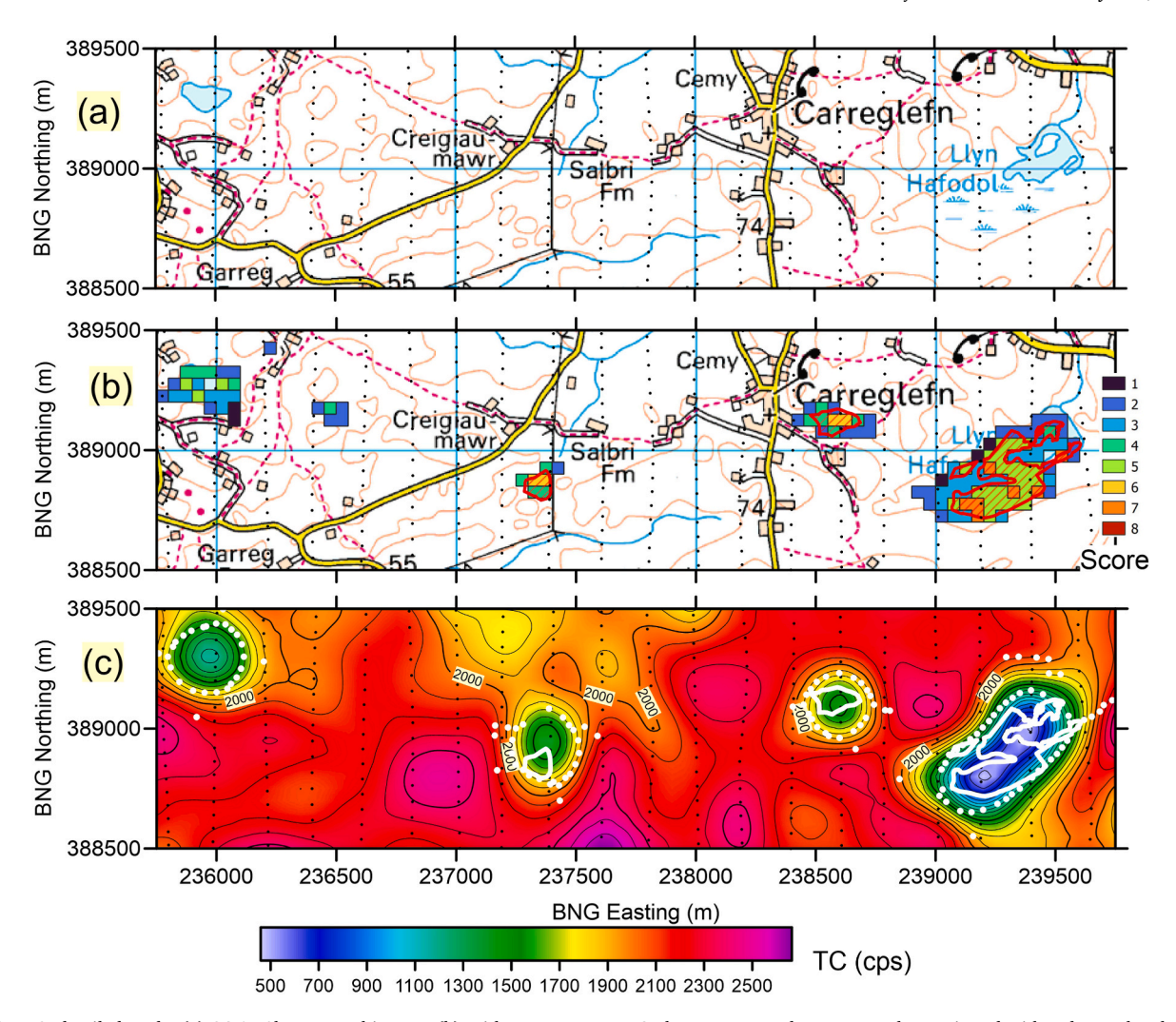


Fig. 6. Area 2, detailed study. (a) OS 1:50k topographic map. (b) With UPMW EVIDENCE layer scores and UNIFIED polygons in red with red cross-hatch. (c) Total Count (TC) image and contours (interval 100 cps) with HGM curvature ridge solutions, (HGM  $\geq$  2.5 cps.m $^{-1}$ ), white dots. UNIFIED polygons in white. The map contains OS data © Crown copyright and database rights 2025. OS AC0000824781 EUL. (For interpretation of the references to colour in this figure legend, the reader is referred to the Web version of this article.)

the 5 main EVIDENCE zones provide attenuation responses with the highest attenuation (about 500 cps) observed across the largest (easternmost) area of peat. Being a moving-average response, the minimum is the best representation of the centre of the source area geometry and the two easternmost UNIFIED layer polygons confirm this. The easternmost polygon demonstrates the smooth response of the data to a complex geometrical source area. In summary, the example demonstrates the confirmation of three peat zones defined by the UNIFIED layer together with an additional zone identified only within the EVIDENCE layer.

#### 5.2.3. Area 3

Area 3 presents a more complex larger area (3.25  $\times$  3.5 km). The area contains 3 SSSI sites (Sites of Special Scientific Interest) which form part of the Anglesey Fens. The wetlands are all, to varying degrees, dependent upon the quality and quantity of groundwater input to maintain their hydrological functioning. The area contains one conventional peat as indicated in Fig. 7a.

Fig. 7b shows the EVIDENCE layer grid and is also overlaid with the UNIFIED layer polygons. Much of the conventional peat area has been assigned a score of 1 and as a consequence the area of UNIFIED defined peat is much reduced from that of the conventional peat. The CF fen does not generate a UNIFIED polygon (probably an error). Fig. 7c shows the THICKNESS and UNIFIED layers. The two small UNIFIED polygons of peat in the west have a low THICKNESS value of 0–42 cm. Finally Fig. 7d

shows an image of the TC data with the curvature (ridge) solutions obtained from the HGM grid. Here the ridge solutions are shown with a threshold of HGM $\geq$ 1.5 cps.m $^{-1}$ . The UNIFIED polygons are shown together with the water courses from the NRW river database (in blue); these appear more limited than those shown on the OS 1:50k topographic maps in the previous panels. A number of attenuation zones at TC < 1500 cps are observed. The zone associated with the CB fen site shows a good agreement with the UNIFIED polygons and the CF fen site (no UNIFIED polygon) response is exceptional (generating a clear low amplitude) for such a small zone. In the NE, the GR fen provides two responses associated with the UNIFIED polygons but indicates a larger extent of the main zone. The curvature ridge solutions, using the low threshold, can be seen to respond to a number of spatial gradients (enhanced amplitudes) in the non-peat soils. The large attenuation zone in the north is comparable to the main GR fen response and is not identified in the EVIDENCE layer and so represents a new potential peat zone. Three small zones of attenuation appear to the NW of the CF fen with only the western-most identified within the UNIFIED layer. By association, the other 2 zones might also be interpreted as thin peats.

#### 5.2.4. Area 4

Since much of the study area contains many inter-tidal and coastal zone influences, an example is presented from a low-lying area. The 3.5  $\times$  4 km area lies at the north-eastern margin of Maltreath Marsh (Fig. 2).

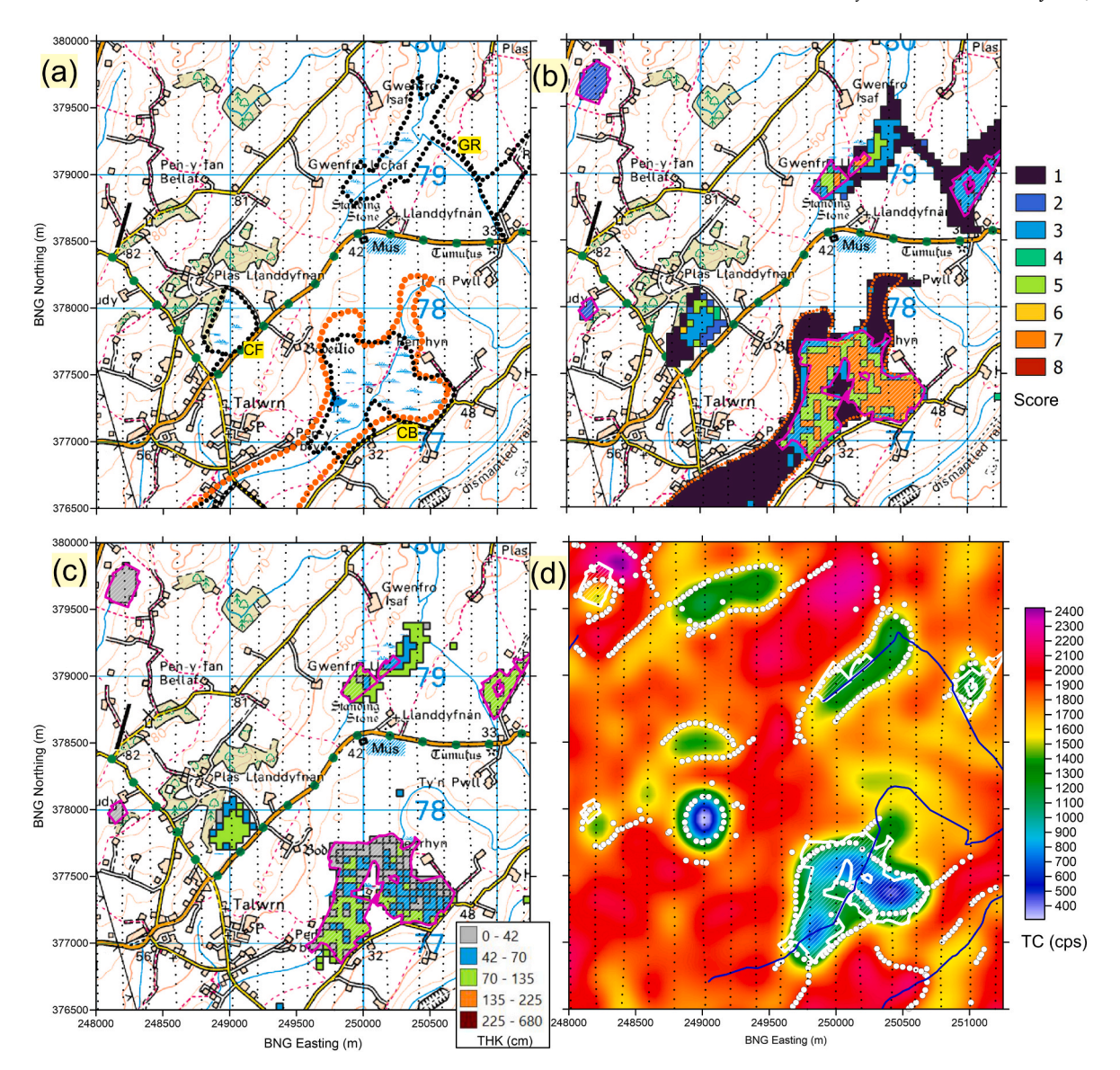


Fig. 7. Area 3, detailed study. (a) OS 1:50k topographic map with conventional peat polygon in orange dots. Three SSSI sites (Sites of Special Scientific Interest) outlined with black dots. These are Cors Bodeilio (CB), Cors y Farl (CF) and Gwenfro and Rhosy Gad (GR). (b) With UPMW EVIDENCE layer scores and UNIFIED polygons in purple with white cross-hatch. Conventional peat polygon in small orange dots. (c) With UPMW THICKNESS (THK) layer and UNIFIED polygons in white. (d) Total Count (TC) image with HGM curvature ridge solutions (HGM  $\geq$  1.5 cps.m $^{-1}$ ), white dots. UNIFIED polygons in white. NRW water courses in blue. The map contains OS data © Crown copyright and database rights 2025. OS AC0000824781 EUL. (For interpretation of the references to colour in this figure legend, the reader is referred to the Web version of this article.)

The whole of this extensive marsh area was studied using the airborne electromagnetic data in connection with saline incursion by Beamish (2012). Fig. 8a shows the area with the outline of a single purple polygon of the UNIFIED peat layer. A topographic trough is partially defined by the lowest (10 m) contour. The canalised Afon Cefni strikes NE through the centre of the trough where elevations are below 2 m. It continues below the road and rail bridges to enter a marsh area and then the UNIFIED peat zone. Fig. 8b shows an image of the TC data with a single black contour identifying TC = 1500 cps. Also shown is the 5 m topographic contour and the NRW water course layer which differs, in detail, from the OS 1:50k map equivalent (Fig. 8a). An attenuation zone is clearly associated with the peat zone. By association we could suggest that the attenuation zone(s) in the SW may also indicate peat. This zone extends in a semi-continuous fashion to the NE for about 3 km as identified by the 1500 cps single contour. We note that this same attenuation level has been used in the previous examples to confirm peat defined by the EVIDENCE and UNIFIED control layers.

Fig. 8c assembles the results of the previous panel over a shadedrelief image of the Lidar DTM. There are two soil types associated with the trough floor and both, as expected, are associated with naturally high groundwater. The soil units on the flanking higher ground are described as freely-draining. The single TC = 1500 cps contour (yellow) is carried across from the previous panel. We also show the HGM curvature ridge solutions at two levels,  $HGM = 2.0-2.5 \text{ cps.m}^{-1}$  (cyan) and HGM 2.5–10 cps.m<sup>-1</sup> (white). The UPMW peat (white polygon) is well defined but with a smaller extent. An additional zone of potential peat, immediately to the west of a prominent drumlin and the main peat, is also identified. Well defined ridge solutions are observed in the SW zone of potential peat but are less well defined to the NE where attenuation decreases. We can also note two attenuation features on the higher ground in the east (freely draining soils) and some ridge solutions associated with enhanced and localised amplitude responses. From Fig. 8c it is evident that the main attenuation anomalies lie within the floor of the trough but are confined to extensive but spatially confined

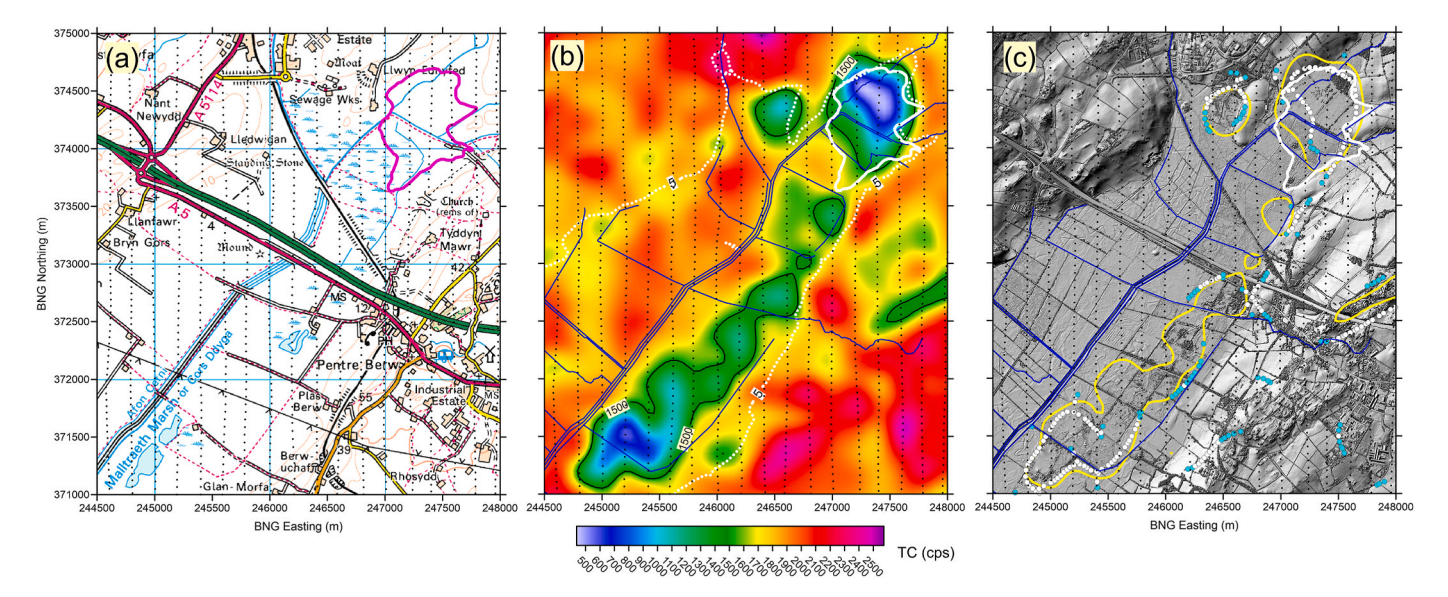


Fig. 8. Area 4, detailed study. (a) OS 1:50k topographic map with UPMW EVIDENCE and UNIFIED peat outlined by purple polygon. (b) Total Count (TC) image with TC = 1500 cps contour shown in black. 5m elevation contour shown in dotted white. UNIFIED peat outlined by white polygon. NRW water courses in blue. (c) Grey shaded relief image of Lidar topography data. UNIFIED peat outlined by white polygon. Total Count (TC) contour TC = 1500 cps contour shown in yellow. HGM curvature ridge solutions HGM 2.25–2.5 cps.m $^{-1}$  shown in cyan, HGM $\geq$ 2.5 in white. NRW water courses in blue. The map contains OS data  $\odot$  Crown copyright and database rights 2025. OS AC0000824781 EUL. (For interpretation of the references to colour in this figure legend, the reader is referred to the Web version of this article.)

zones that incorporate the area identified by the UNIFIED peat layer. We are therefore uncertain as to the BD-SAT interpretation of the majority of these larger attenuation features located in this, and other, coastal zones.

#### 5.2.5. Summary

An overview summary is presented in Fig. 9 which uses the shaded-relief, normalised Local Variance (LV) response of the TC data in grey. The high variance edges detected can be due to high flux contrasts, as at the two quarry locations discussed previously (yellow circles), or low flux as associated with onshore water bodies (shown in white) and at

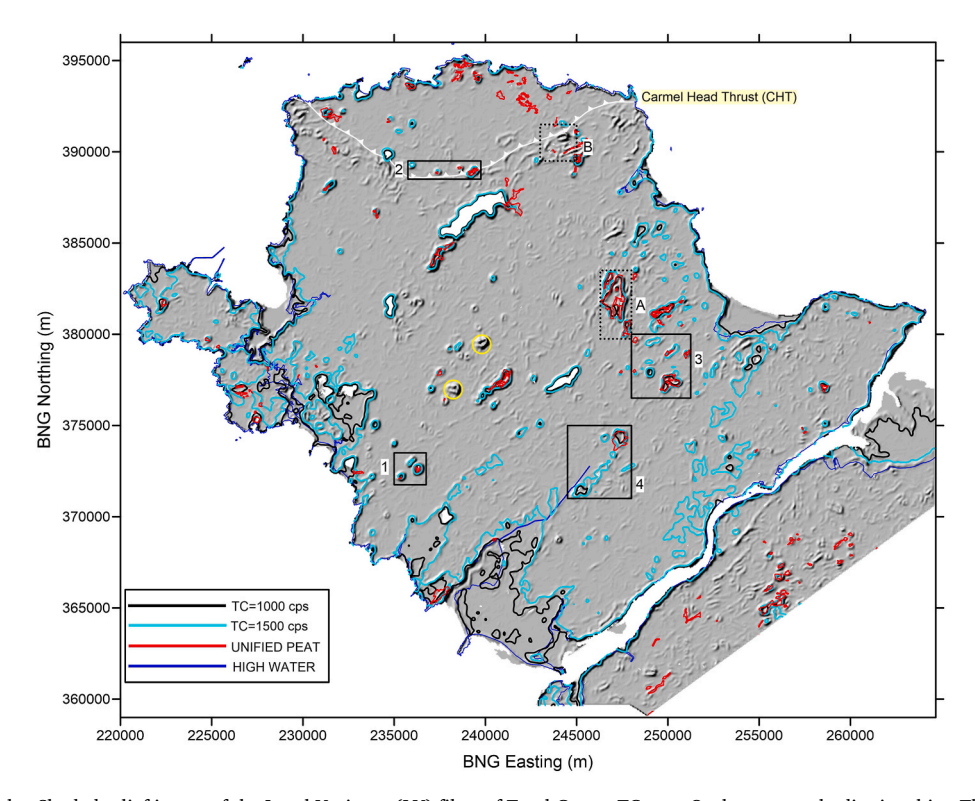


Fig. 9. Summary of results. Shaded relief image of the Local Variance (LV) filter of Total Count, TC, cps. Onshore water bodies in white. The UPMW UNIFIED layer polygons in red. Two high attenuation levels of the TC data are shown by TC = 1000 cps (black) and TC = 1500 cps (cyan). Two yellow circles denote high flux quarries. The blue line denotes the highwater mark. Detailed study rectangles are shown as solid lines (Areas 1–4) and also 2 rectangles (A, B) with dotted lines. (For interpretation of the references to colour in this figure legend, the reader is referred to the Web version of this article.)

peat locations. The unified peat polygons are shown in red. To summarise the main attenuation features we have chosen two contour levels which are TC = 1000 cps which represents high attenuation (or -77 %of the survey median) and TC = 1500 cps which represents -37 % of the survey median (=2380 cps using a reduced data set). The higher value of TC = 1500 cps can be associated with many peat areas in the unified map (detailed study areas 1-4). This level is also associated with many larger scale attenuation effects, similar to those observed in Area 4. Along the northern coast we observe many areas of UNIFIED peat with no attenuation response at the selected level, this is also observed within the mainland portion of the study area. In the area to the NE and east of Rectangle A (Fen peat) we observe a particular clustering of high attenuation zones not identified in the UPMW information. Elsewhere we observe a startling plethora of flux contrasts (edges) detected by the LV response. We have noted a few of these but, since they warrant detailed scale studies, their further assessment is deferred.

#### 6. Discussion

The multi-sensor, airborne survey data described here were intended for both resource and environmental applications. The survey specifications may be considered typical of modern airborne data sets which can achieve both regional and country-wide coverage providing millions of line-km of uniform spatial information. The 6316 line-km of the small Anglesey survey were obtained over 6 survey days plus an additional 1.5 days for the required local calibrations (all sensors). It is clear that a suitable design procedure to provide digital soil mapping involving detailed peat detection could be made by acquiring data at lower elevations and at slower speeds (higher sampling rates). Drone based acquisition systems continue to be developed for such purposes. Heavy lift drones, capable of employing a sufficient volume of crystal packs, have been introduced to the commercial marketplace.

The airborne radiometric data that were acquired globally since the beginning of this century have benefited greatly by the introduction of appropriate and standardised acquisition, calibration and processing procedures that are summarised by IAEA (2003). As drone radiometric surveys come into more routine use, it is important that similar practices are adopted. Lower elevation survey design and the required protocols and procedures differ significantly from existing airborne procedures. Guidelines for their implementation are given by van der Veeke (2023).

The sensitivity of the radiometric response to soil saturation levels is of interest in a wide range of disciplines. Some of the additional influences on the response are termed environmental (e.g. cosmic rays, rainfall and radon). The most accurate and detailed understanding of the radiometric response has come from static monitoring experiments. These can use data integration times of minutes/hours and benefit from detailed control measurements of in-field soil parameters particularly soil moisture which has intermittent together with diurnal/seasonal components. In the static case, the support volume can be adjusted by varying the height of the sensor. Amestoy et al. (2021) employed a 50 m tower height to simulate an airborne measurement and results are presented over a 14-month period. Other, much lower elevation (2.25 m), static experiments are aimed at agricultural crop management (Strati et al., 2018) and indicate that, in detail, the additional water content of the biomass (e.g. the crop) should also be accounted for.

More recently, static testing has been applied to new compact scintillator-based sensors especially designed to jointly measure neutron counts (cosmic ray) together with muons and total gamma rays in relation to soil moisture estimation. The study by Gianessi et al. (2024), compared all 3 approaches and suggested that the radiometric sensors offer a reliable counterpart to the more widely used cosmic ray neutron sensing (CRNS) long-term monitoring systems. The CRNS technique has a certain synergy with the equivalent radiometric technique in that: (i) it employs the cosmic ray neutron showers which are a required correction in the calibration and processing of airborne radiometric data and (ii) it presents a similar large scale support volume to the airborne

measurement

Interpretation of the radiometric BD-SAT response (Fig. 1) would obviously benefit from independent assessments of soil moisture/saturation levels. A number of common procedures and data sets are available to perform these types of assessment. When examining the radiometric attenuation levels we have considered, for example:

- (i) The Copernicus high-resolution Water and Wetness product is an amalgamation of earth observation information including Sentinel −1 and −2 and several other products. The landing page containing links to the data and documentation can be found at <a href="https://land.copernicus.eu/en/products/high-resolution-layer-water-and-wetness">https://land.copernicus.eu/en/products/high-resolution-layer-water-and-wetness</a>. The product provides 5 classes of information ranging from permanently wet to dry. We used the 2015 data set supplied at a resolution of 20 m.
- (ii) The LANDIS® national soil wetness map which is a derived product from the National Soil Map (England and Wales). Six distinct soil wetness classes are defined. The data are described at https://www.landis.org.uk/data/nmwetness.cfm. Soil data © Cranfield University and for the Controller of HMSO 2025.
- (iii) There are a wide number of techniques based on hydrological terrain analysis that use the framework provided by a DTM. Here we investigated the common Terrain Wetness Index using the Lidar 1 m DTM (Mattivi et al., 2019).

Although undoubtedly useful in certain applications, we found that the information provided by these approaches did not provide any specific relevant control in the relation to the observed radiometric attenuation information.

#### 7. Conclusions

Using a recent airborne survey across Anglesey, North Wales, the focus of our study has been on the geophysical, property-based detection of peat and peaty soils using the control provided by a new, observational, evidence-based approach to peat mapping and hence carbon accounting. The new mapping identifies many small pockets of the carbon store which can be termed the lost peatlands, unaccounted for in previous assessments. The information is used to provide interpretation control of the many localised attenuation zones observed across our study area. By spatial colocation between the radiometric data and peat map we are then confident that the attenuation zones identify a peat response.

We have presented a revised and simplified radiometric attenuation theory for all soils. The theory can be applied to any form of radiometric survey data. It can be used to readily understand the high detectability of peat and peaty soils in the context of their property contrasts with adjacent soils. It also provides a framework for understanding the continuum of radiometric responses (both attenuation and enhancement) across all soils which we routinely observe but have yet to interpret. Localised high values of flux are evident in all 4 of the detailed study areas and are presumed to be soil related. According to Fig. 1, these zones are concomitant with a relative increase in bulk density (e.g. reduced carbon content) and/or a decrease in degree of water saturation.

We have pointed out the dual soil properties of bulk density and water saturation (BD-SAT) which combine to form the observed attenuation behaviour. Knowledge of these properties is ultimately required across the large support volume of airborne measurements.

To examine the high-wavenumber content of the radiometric data sets we introduced the Local Variance (LV) filter. This does not appear to have used previously in the geophysical literature but is a straightforward and robust procedure to apply to any data set. The LV behaviour of the normalised %K, eTh, eU and the Total Count (TC) data allows a qualitative comparison of the different, high wavenumber, signal-to-noise contributions. For our data set the TC data appear least prone to

noise while the eU behaviour is distinctly noisy. When used at the detailed scale, the LV response provides a robust surrogate to the edge detection procedures requiring the calculation of spatial gradients.

Using the TC data and the new updated peat map of Wales we have provided both large-scale and detailed comparisons of the many attenuation zones observed and the evidence for peat. The evidence layer, when translated to a unified peat map, comprises 162 polygons of small spatial extent (128 are  $<0.05 \text{ km}^2$ ). This results in primary attenuation responses often confined to 1 or 2 adjacent survey lines. We know from previous modelling studies that when such zones are less than the line spacing (200 m) the correct attenuation level is not achieved. This results from the large support volume at the airborne measurement height (52-54 m in our case). The large support volume also introduces a moving spatial averaging of the along-line data. The outcome is a smoothing (low pass filtering) of the attenuation response which is confirmed in our detailed studies. The smoothing also translates to the edge-detection procedures used here which often adopt circular forms. Larger zones (e.g. ≫ 200 m) do however adopt more realistic geometrical forms in keeping with the control evidence layer.

Despite the spatial limitations described here, the attenuation response appears sufficient to either confirm or reject the evidence for a zone of peat. In addition, the airborne data suggest many other areas of potential peat which may not have entered the evidence database. When summarising the attenuation across the whole survey area (Fig. 9), we have chosen two contour levels which are TC=1000 cps (high attenuation, or -77 % of the survey median) and TC=1500 cps which represents -37 % of the survey median. The latter can be associated with many peat areas in the unified map (detailed study areas 1–4). This level is also associated with many larger scale attenuation effects, similar to those observed in Area 4. We suggest these areas warrant further study in relation to the dual BD-SAT soil properties.

#### CRediT authorship contribution statement

**David Beamish:** Writing – original draft, Formal analysis, Conceptualization. **James C. White:** Writing – review & editing, Project administration.

# Declaration of competing interest

The authors declare that they have no known competing financial interests or personal relationships that could have appeared to influence the work reported in this paper.

#### Acknowledgements

We thank Sam Roberson for internal BGS reviewing. The required copyright acknowledgements used in this study are provided in each of the Material descriptions of Section 3. As is clearly indicated, much of the material across Anglesey forms part of a Welsh Government Open Government Licence for Public Sector Information. Contains public sector information licensed under the Open Government Licence v3.0. This research did not receive any specific grant from funding agencies in the public, commercial or not-for-profit sectors. This paper is published with the permission of the Executive Director, British Geological Survey (NERC).

#### Appendix A. Supplementary data

Supplementary data to this article can be found online at https://doi.org/10.1016/j.jenvrad.2025.107858.

#### Data availability

The material data sources used in this study are identified and described in each of the Material descriptions of Section 3.

#### References

- Adams, W.A., 1973. The effect of organic matter on the bulk and true densities of some uncultivated podzolic soils. J. Soil Sci. 24, 10–17. https://doi.org/10.1111/j.1365-2389.1973.tb00737.x.
- ADAS, 2019. Review of best practice for SOC monitoring. Soil Policy Evidence
  Programme Report: SPEP 2019-20/05. Soil Policy & Agricultural Land Use Planning
  Unit, Land, Nature and Forestry Division. Department for Rural Affairs. Welsh
  Government. https://gov.wales/sites/default/files/publications/2020-11/assessme
  nt-soil-issues-in-context.pdf.
- Altfelder, S., Preugschat, B., Matos, M., Kandzia, F., Wiens, B., Eshmuradov, O., Kunze, C., 2024. Upscaling ground-based backpack gamma-ray spectrometry to spatial resolution of UAV-based gamma-ray spectrometry for system validation. J. Environ. Radioact. 273, 107382, https://doi.org/10.1016/j.jenyrad.2024.10738.
- Amestoy, J., Meslin, P.-Y., Richon, P., Delpuech, A., et al., 2021. Effects of environmental factors on the monitoring of environmental radioactivity by airborne gamma-ray spectrometry. J. Environ. Radioact. 237, 106695. https://doi.org/10.1016/j. ienvrad.2021.106695.
- Beamish, D., 2012. A study of saline incursion across an inter-tidal zone on anglesey, Wales using airborne conductivity data. Near Surf. Geophys. 10 (2), 171–184. https://doi.org/10.3997/1873-0604.2011048.
- Beamish, D., 2013. Gamma ray attenuation in the soils of Northern Ireland, with special reference to peat. J. Environ. Radioact. 115, 13–27. https://doi.org/10.1016/j. jenvrad.2012.05.031.
- Beamish, D., 2014. Peat mapping associations of airborne radiometric survey data. Remote Sens. 6 (1), 521–539. https://doi.org/10.3390/rs6010521.
- Beamish, D., 2015. Relationships between gamma-ray attenuation and soils in SW England. Geoderma 259–260, 174–186. https://doi.org/10.1016/j.geoderma.2015.05.018.
- Beamish, D., 2016a. Soils and their radiometric characteristics. In: Young, M.E. (Ed.), Unearthed: Impacts of the Tellus Surveys of the North of Ireland. Royal Irish Academy, Dublin. https://nora.nerc.ac.uk/id/eprint/515923/1/Chapter19.pdf.
- Beamish, D., 2016b. Enhancing the resolution of airborne gamma-ray data using horizontal gradients. J. Appl. Geophys. 132, 75–86. https://doi.org/10.1016/j. jappgeo.2016.07.006.
- Beamish, D., Busby, J., 2016. The Cornubian geothermal province: heat production and flow in SW England: estimates from boreholes and airborne gamma-ray measurements. Geotherm. Energy 4 (4), 25. https://doi.org/10.1186/s40517-016-0046-8.
- Beamish, D., Farr, G., 2013. Airborne geophysics: a novel approach to assist hydrogeological investigations at groundwater-dependent wetlands. Q. J. Eng. Geol. Hydrogeol. 46 (1), 53–62. https://doi.org/10.1144/qjegh2012-019.
- Beamish, D., Schofield, D.I., 2010. HiRes airborne geophysical survey of Anglesey: a key dataset for unravelling complex geology and establishing an environmental baseline. In: Geological Society of America Joint Meeting, Baltimore, USA, 14-16 March 2010. Geological Society of America, Baltimore, USA [Poster]. https://nora.nerc.ac.uk/id/eprint/529963/1/Anglesey\_A0\_poster\_GSA\_Abstracts\_MARCH\_2010.pdf.
- Beamish, D., White, J.C., 2009. The Hires Airborne Geophysical Survey of Anglesey: Logistics Report. British Geological Survey, Nottingham, UK, p. 31. IR/09/061. htt ps://nora.nerc.ac.uk/id/eprint/518965/.
- Beamish, D., White, J.C., 2011. Aeromagnetic data in the UK: a study of the information content of baseline and modern surveys across Anglesey, North Wales. Geophys. J. Int. 184 (1), 171–190. https://doi.org/10.1111/j.1365-246X.2010.04852.x.
- Beamish, D., White, J.C., 2024. On the detailed mapping of peat (raised bogs) using airborne radiometric data. J. Environ. Radioact. 277, 107462. https://doi.org/10.1016/j.jenvrad.2024.107462.
- Billings, S.D., Minty, B.R., Newsam, G.N., 2003. Deconvolution and spatial resolution of airborne gamma-ray surveys. Geophysics 68 (4), 1257–1266. https://doi.org/ 10.1190/1.1598118.
- British Geological Survey, 2005. Digital Geological Map of Great Britain 1:250 000 Scale (DiGMapGB-250) Data. Version 4.11. British Geological Survey, Keyworth, Nottingham. Tile SH. Release data 15.11.05.
- Duval, J.S., Cook, B., Adams, J.A.S., 1971. Circle of investigation of airborne gamma-ray spectrometer. J. Geophys. Res. 76, 8466–8470. https://doi.org/10.1029/ 1007502466
- England, J.R., Viscarra Rossel, R.A., 2018. Proximal sensing for soil carbon accounting. Soil 4, 101–122. https://doi.org/10.5194/soil-4-101-2018.
- Farewell, T.S., Truckell, I.G., Keay, C.A., Hallett, S.H., 2011. The use and applications of the soilscapes datasets. National Soil Resources Institute. Cranfield University. https://dspace.lib.cranfield.ac.uk/items/0b08c717-57b4-42f0-ae31-ec6f735cf3b2.
- Gianessi, S., Polo, M., Stevanato, L., Lunardon, M., Francke, T., Oswald, S.E., Said Ahmed, H., Toloza, A., Weltin, G., Dercon, G., Fulajtar, E., Heng, L., Baroni, G., 2024. Testing a novel sensor design to jointly measure cosmic-ray neutrons, muons and gamma rays for non-invasive soil moisture estimation. Geosci. Instrum. Method. Data Syst. 13, 9–25. https://doi.org/10.5194/gi-13-9-2024.
- Gilet, L., TMorley, T.R., Flynn, R., Connolly, J., 2024. An adaptive mapping framework for the management of peat soils: a new Irish peat soils map. Geoderma 447, 116933. https://doi.org/10.1016/j.geoderma.2024.116933.
- IAEA, 2003. Guidelines for Radioelement Mapping Using Gamma Ray Spectrometry. International Atomic Energy Agency, Vienna. Technical Report Series, No. 136. https://www-pub.iaea.org/MTCD/Publications/PDF/te\_1363\_web.pdf.
- IAEA, 2013. Advances in airborne and ground geophysical methods for Uranium exploration. IAEA Nuclear Energy Series NF-T-1 5. https://wwwpub.iaea.org/ MTCD/Publications/PDF/Pub1558\_web.pdf.

- IUCN, 2023. IUCN UK peatland programme. Use of peat depth criteria: accounting for the lost peatlands. https://www.fensforthefuture.org.uk/admin/resources/do wnloads/use-of-peat-depth-criteria-accounting-for-the-lost-peatlands1.pdf.
- Joint Nature Conservation Committee, 2011. Towards an Assessment of the State of UK Peatlands. JNCC. https://hub.jncc.gov.uk/assets/f944af76-ec1b-4c7f-9f62-e47 f68cb1050.
- Lindsay, R., 2010. Peatbogs and carbon: a critical synthesis to inform policy development in oceanic peat bog conservation and restoration in the context of climate change. In: Environmental Research Group. University of East London. https://repository.uel.ac. uk/item/862y6.
- Lourenco, M., Fitchett, J.M., Woodborne, S., 2023. Peat definitions: a critical review. Prog. Phys. Geogr. Earth Environ. 47 (4), 506–520. https://doi.org/10.1177/ 03091333221118353.
- Mattivi, P., Franci, F., Lambertini, A., Bitelli, G., 2019. Open Geospatial Data, Software and Standards 4, 6. https://doi.org/10.1186/s40965-019-0066-y.
- Morgan, L.A., 2012. Geophysical characteristics of volcanogenic massive sulphide deposits in volcanogenic massive sulphide occurrence model. U.S. Geol. Survey Sci. Invest. Rep. 2010-5070-C.
- Périé, C., Ouimet, R., 2008. Organic carbon, organic matter and bulk density relationships in boreal forest soils. Can. J. Soil Sci. 88, 315–325. https://doi.org/ 10.4141/CJSS06008.
- Phillips, J.D., Hansen, R.O., Blakely, R.J., 2007. The use of curvature in potential-field interpretation. Explor. Geophys. 38, 111–119. https://doi.org/10.1071/EG07014.
- Phillips, E., Everest, J., Diaz-Doce, D., 2010. Bedrock controls on subglacial landform distribution and geomorphological processes: evidence from the late devensian Irish Sea Ice Stream. Sediment. Geol. 232, 98–118. https://doi.org/10.1016/j. sedgeo.2009.11.004.
- Pires, L.F., 2018. Soil analysis using nuclear techniques: a literature review of the gamma ray attenuation method. Soil Tillage Res. 184, 216–234. https://doi.org/10.1016/j. still.2018.07.015.
- Pitkin, J.A., Duval, J.S., 1980. Design parameters for aerial gamma ray surveys. Geophysics  $45,\,1351-1441$ .
- Reynolds, W.D., Nurse, R.E., Phillips, L.A., Drury, C.F., Yang, X.M., Page, E.R., 2020. Characterizing mass–volume–density–porosity relationships in a sandy loam soil amended with compost. Can. J. Soil Sci. 100, 289–301. https://doi.org/10.1139/ciss-2019-0149.
- Roberts, M.J., Scourse, J.D., Bennell, J.D., Huws, D.G., Jago, C.F., Long, B.T., 2011. Late Devensian and Holocene relative sea-level change in North Wales, UK. J. Quat. Sci. 26, 141–155. https://doi.org/10.1002/jqs.1443.

- Robinson, D.A., Thomas, A., Reinsch, S., et al., 2022. Analytical modelling of soil porosity and bulk density across the soil organic matter and land-use continuum. Sci. Rep. 12, 7085. https://doi.org/10.1038/s41598-022-11099-7.
- Rühlmann, J., Körschens, M., Graefe, J., 2006. A new approach to calculate the particle density of soils considering properties of the soil organic matter and the mineral matrix. Geoderma 130, 272–283. https://doi.org/10.1016/j.geoderma.2005.01.024.
- Rühlmann, J., 2020. Soil particle density as affected by soil texture and soil organic matter: 1. Partitioning of SOM in conceptional fractions and derivation of a variable SOC to SOM conversion factor. Geoderma 375, 114542. https://doi.org/10.1016/j. geoderma.2020.114542.
- Rhymes, J., Chadwick, D.R., Williams, A.P., et al., 2023. Evaluating the accuracy and usefulness of commercially-available proximal soil mapping services for grassland nutrient management planning and soil health monitoring. Precis. Agric. 24, 898–920. https://doi.org/10.1007/s11119-022-09979-z.
- Strati, V., Albéri, M., Anconelli, S., Baldoncini, M., Bittelli, M., Bottardi, C., Chiarelli, E., Fabbri, B., Guidi, V., Raptis, K.G.C., et al., 2018. Modelling soil water content in a tomato field: proximal gamma ray spectroscopy and soil—crop system models. Agriculture 8, 60. https://doi.org/10.3390/agriculture8040060.
- Thurston, J.B., Brown, R.J., 1994. Automated source-edge location with a new variable pass-band horizontal-gradient operator. Geophysics 59, 546–554. https://doi.org/10.1190/1.1443615
- van der Veeke, S., 2023. UAV-borne Radioelement Mapping: towards a Guideline and Verification Methods for Geophysical Field Measurements. University of Groningen. https://doi.org/10.33612/diss.261264637 [Thesis fully internal (DIV), University of Groningen].
- Welsh Government, 2022. Production of the peatlands of Wales map, soil policy evidence programme, 2020-21. Report code: SPEP2020-21/03. https://www.gov.wales/production-peatlands-wales-map.
- White, J.C., Beamish, D., 2010. The Hires Airborne Geophysical Survey of Anglesey: Processing Report. British Geological Survey, Nottingham, UK, p. 41. OR/10/002. https://nora.nerc.ac.uk/id/eprint/9889/1/OR10002.pdf.
- White, J.C., Beamish, D., 2014. A lithological assessment of the resistivity data acquired during the airborne geophysical survey of Anglesey, North Wales. Proc. Geologists' Assoc. 125 (2), 170–181. https://doi.org/10.1016/j.pgeola.2014.01.003.
- Woodcock, C.E., Strahler, A.H., 1987. The factor of scale in remote sensing. Remote Sens. Environ. 21, 311–332. https://doi.org/10.1016/0034-4257(87)90015-0.